Geologic incoherence index for seismic inversion

Luiz Alberto Santos, PETROBRAS
Webe J. Mansur, Universidade Federal do Rio de Janeiro
George A. McMechan, University of Texas at Dallas

This paper was prepared for presentation during the 13th International Congress of the Brazilian Geophysical Society held in Rio de Janeiro, Brazil, August 26-29, 2013.

Abstract

The velocity field necessary to map events into their correct positions during migration does only need to honor the kinematic behavior of the subsurface. Such velocity field, if no constraint is imposed, does not have any compromise with the reality. In this work we propose the Geologic Incoherence Index (GII) to obtain geologically feasible models during any inversion process. The technique is presented in a tomographic inversion over common focusing operators (CFPO) in a synthetic model.

Introduction

It is often stated that an inverse problem has a unique solution if, when the model changes from **m1** to **m2**, the data also change from **d1** to **d2**, in such a way that **d1** and **d2** are different (Sen, 2006). Non-uniqueness of solution is an undesired characteristic of inverse problems. Thus, it is important to know the nature and the general characteristics of the model to reduce the multiple solutions of the inverse problem. The a priori knowledge of the model **m** guides the best way to represent it by the use of constraints imposed into an inversion process. Consider of the most fundamental units of a sedimentary basin (the rocks) is revisited. A rock is any coherent, solid aggregate of minerals that constitute a planet (Skinner and Porter, 1987). A mineral is a substance with defined chemical composition and crystalline structure formed by natural processes.

Beyond minerals, rocks have pores, that are the intergranular spaces. Given a rock sample, its porosity is defined as the ratio between the void volume and the total volume (Mavko et al., 2009). In a geological medium, the sedimentary rocks have their pores filled by fluids (air, brine, fresh water, gas and/or oil). The main intrinsic factors that determine the physical properties of rocks are their mineral composition, the intergranular contact shape, the grain shape, the porosity, and the interstitial fluids (their composition and pore-pressure). External factors such as temperature and confining (lithostatic) pressure also have strong influence in the velocity of lithotypes (Mavko et al., 2009 and Thomas, 2000). Temperature tends to reduce the P velocity and also the elastic modulus as the temperature rises. Increasing the confining pressure increases the velocity as it reduces the porosity; as compaction increases for a single lithology, the P velocity also increases.

Because of the variables cited in the previous paragraph, a single lithology can have a large range of P velocity variation. In Mavko et al. (2009) and Carmichael (1982), there are extensive lists of P velocities for several lithotypes under different temperature, pressure and fluid saturation conditions. Sedimentary rocks are formed by sediments deposited as layers. A layer is a rock (or sediment) interval with upper and lower bounding interfaces which are usually a depositional hiatus, or an erosional period (Park, 1989). Sheriff (2002) defines a layer as an interval whose properties differ from what is beneath and above. Park's definition has a genetic meaning, and informs the cause of layer distinction, while Sheriff's expresses the consequences in terms of layer properties. Seismic waves are sensitive to mechanical property contrasts that cause reflections at interfaces. The original atitude (the dip and strike, Sheriff (2002)) of sedimentary rocks, or layering, are dominantly horizontal or sub-horizontal.

Because of the flow conditions of a specific depositional environment, a single layer may have lateral changes in properties or facies. These changes can be in the lithology, sedimentary structures, grain size, etc. (Sheriff, 2002). During the geologic evolution, sedimentary rocks can experience deformation episodes of different origins (tectonic or not) and intrusions (igneous, salt or mudstone), that change the original geometry of the strata and causes folds and faults.

Geological Incoherence Index

Sedimentary rocks are mainly distributed as layers, deformed or not, and because of the compaction, it is expected that density increases with depth for a single porous lithology. By using the premise that, for a porous medium, velocity is proportional to density, velocity also increases with depth for a rock of homogeneous composition.

In Figure 1a, there is a raw velocity log of a thick section of a Brazilian sedimentary basin. Figure 1b shows the low frequency version of the curve in Figure 1a and it represents the compaction trend. For a non-deformed to gently deformed sedimentary pile, the low frequency velocity curve increases (Figure 1b) from the top to the bottom in the same layer.

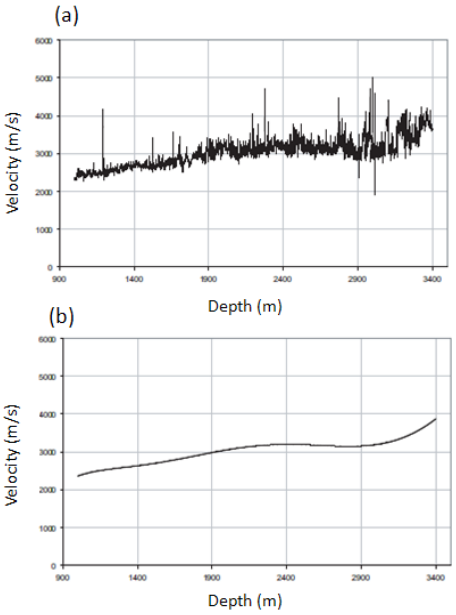

Figure 1: Velocity x depth curve with original data (a) and the low spatial frequency filtered version (b).

Because of the sedimentation conditions and post-depositional diagenesis, the velocity gradient may be parallel to the gravity, orthogonal to an equipotential surface. For flat bedrock conditions, the vector of maximum velocity increase is orthogonal to the layer bottom. For a sedimentary sequence inside of which there is no episode of erosion or deformation, the velocity gradient vector tends to be parallel either to the top or bottom normal of the same layer.

Now that the premises of the relation between the layer and the velocity field are set, it is possible to quantify a geological incoherence index (GII) that may be computed as follows. First the gradient of the velocity field (v) must be computed by

$$\nabla v = \left(\frac{\partial v}{\partial x}, \frac{\partial v}{\partial z} \right) \qquad (1).$$

Then the angle θ_v that the gradient vector makes with the horizontal is calculated by

$$\theta_v = \arctan\left(\frac{\frac{\partial v}{\partial z}}{\frac{\partial v}{\partial x}} \right) \qquad (2).$$

Next, the normal vector of each point of the layer's interface is calculated. The angle of those normal vector are calculated and extrapolated for each corresponding layer. Either the top or the bottom interface may be used to proceed to the extrapolation to inside the stratum. When the extrapolation is done for the entire model discretized by grid, there is another field θ_s that has a similar meaning to θ_v.

According to the premises cited above, θ_s should be equal to θ_v. The GI index is computed by

$$GII = \frac{\sum_{i=1}^{n} abs(\theta_{v,i} - \theta_{s,i})}{n} \qquad (3).$$

where n is the number of cells of the model.

By computing $\theta_{v,i}$ and θ_{si} ranging from 0 to 180 degrees, the most incoherent situation is the one that $\theta_{v,i}$ and $\theta_{s,i}$ are orthogonal in each cell. In this case GII reaches the maximum value of 90 degrees. If, otherwise, $\theta_{v,i}$ and $\theta_{s,i}$ are parallel in the entire model, GII has its minimum value of zero. Then, GII ranges from 0 to 90 for respectively lowest and highest incoherence. The analysis comparing sets of models may be done for the same grid cells. In Figure 2a there is a model represented by a layer limited at its top and bottom by horizontal surfaces and the velocity field shows a vertical gradient. $\theta_{v,i}$ and $\theta_{s,i}$ are computed and shown in Figures 2b and 2c. IIG, calculated with equation 3, is 0^o. For the model in Figure 2d the layer boundaries are the same as in 2a, but the velocity gradient show only lateral changes. Thus for 2d, the $\theta_{v,i}$ and $\theta_{s,i}$ are respectively in Figures 2e and 2f, causing an IIG of 90^o. The model in Figure 2a is more geologically reasonable than the one in Figure 2d.

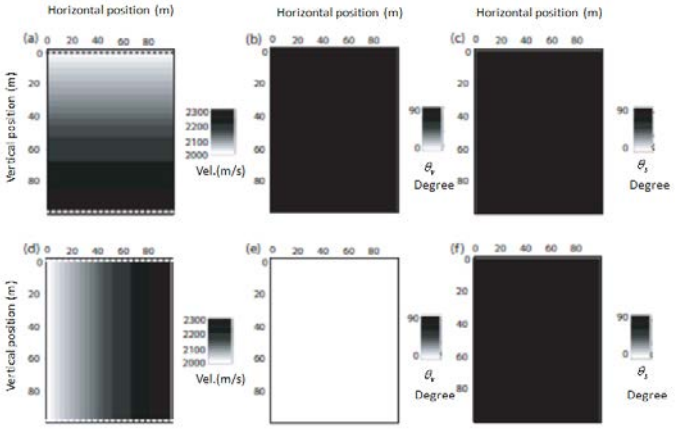

Figure 2: a) Vertically changing velocity model in a layer limited by horizontal top and bottom surfaces; b) Dip of the gradient of the model at (a), θ_v; c) Top surface normal dip of the model at (a), θ_s; d) Horizontally changing velocity model of a layer limited by horizontal top and bottom surfaces; e) Dip of the gradient of the model at (d), θ_v; f) Top surface normal dip of the model at (d), θ_s.

Use of GII in sequential tomographic inversion

Given a synthetic dataset of common focus point operators (CFPO) (Berkhout, 1989), obtained from the model at Figure 3, we perform a two step tomographic inversion with two approaches to recover the original model.

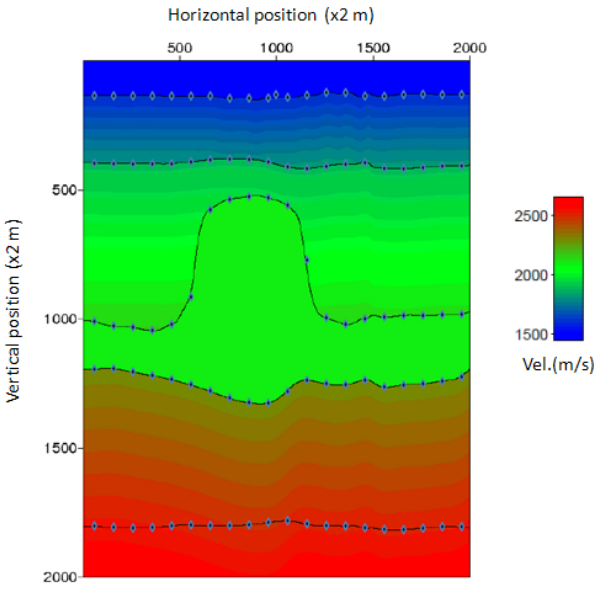

Figure 3: Original velocity and strucutural model

In both approaches the first step consist in perform tomographic inversion using the layer-stripping approach. In a second step we perform the inversion using two different parameterizations, described as follows.

Step 1: Tomographic inversion using layer stripping with 1D spline parameterization

For the first step the CFPOs that define the base of the shallowest layer, layer one, are used to determine the velocity of this layer and the shape of its bottom. Then the CFPOs that define the bottom of the layer below layer 1 are used in another inversion. This process is repeated until the deepest interface is reached. Each layer is parameterized using 1D spline functions delivering laterally changing velocity field.

For the layer stripping inversion a homogeneous velocity model of 1500 m/s was used for the first layer and its bottom is positioned at 400 m depth. After the estimation of the velocity field of each layer, the average is used to estimate the a priori velocity for the next deeper layer. No constraints or regularization are used at any layer. It took 5, 6, 10, 6 and 17 iterations for layers 1, 2, 3, 4 and 5 respectively to converge to the model in Figure 4. The relative residuals for layers 1, 2, 3, 4 and 5 are 0.00119491, 0.0010786, 0.00258387, 0.00216280 and 0.00398514 s respectively. The total error (equation 3) is 4.4853e+10 m/s and the GII is 66.70.

$$\varepsilon_t = \frac{1}{n}\sum_{i=1}^{n}\left|m_{real,i} - m_{calc,i}\right| \qquad (3)$$

Where ε_t is total error, n is the number of cells of the model, $m_{real,i}$ and $m_{calc,i}$ are the i^{th} cell of the real and estimated models respectively.

The high GII indicates that, despite of the low residual, it is an unrealistic result. It is a good kinematically equivalent model (KEM), and so can be used for seismic migration, but no other dynamic information can be extracted.

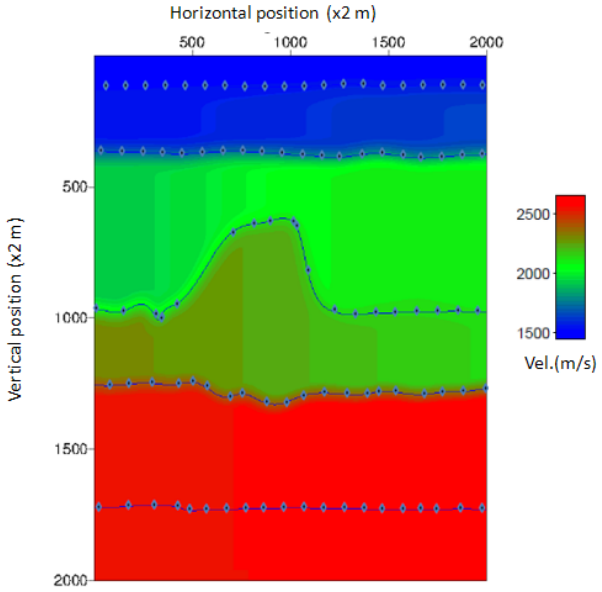

Figure 4: Velocity and structural model estimated with layer stripping approach using 1D splines parameterization for the velocity field at each layer.

Step 2: Second tomographic inversion using different parameterizations

In the next two examples below, the layer stripping and global inversion are used for the second tomographic step and the input, or a priori, model is the result of layer stripping described in the step 1, Figure 4. For the example A, the equation 4 is employed to represent the velocity field in the layer-stripping approach, a mathematical model that is suitable to represent layering of sedimentary rocks concordant to the upper boundary of a layer. This is the top-concordant parameterization.

$$v_j(x,z) = v_{0,j} + \left\lfloor z_{top,j}(x) - z \right\rfloor B_j \qquad (4)$$

Where $z_{top,j}$ is the top boundary of j^{th} layer, z is vertical coordinate inside the layer, $v_{0,j}$ is the velocity at $z_{top,j}$ and B_j is the vertical gradient.

In example B a 2D spline parameterization is used describing the entire model. In such approach the entire model is inverted in each iteration.

In example A the inversion converged to the model in Figure 5 after 22 iterations with residuals of 0.00110168, 0.000997521, 0.00287459, 0.00216722 and 0.00187692 s for layers 1, 2, 3, 4 and 5 respectively. The total error (equation 3) is equal to 3.05589e+10 m/s and GII is 24.22. During the iterations, the main changes occur in the velocity field.

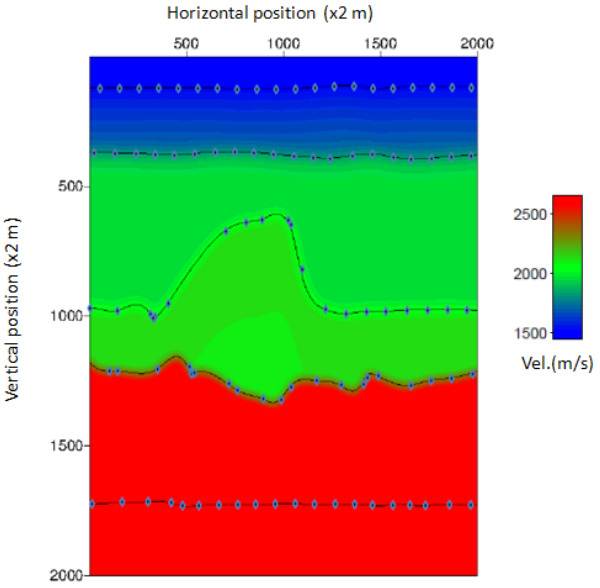

Figure 5: Velocity and structural model estimated with layer stripping approach using equation 4 for parameterization of the velocity field at each layer.

For example B, after 14 iterations, the inversion converged to the model at Figure 6, a residual of 0.001712 s, a total error (equation 3) of 2.45407e+10 m/s and a GII of 21.55. During the iterations, the structural model did not change much, but the velocity field did.

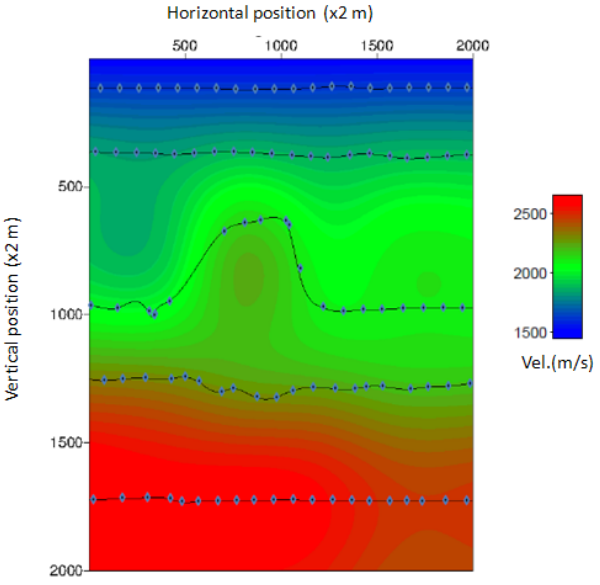

Figure 6: Velocity and structural model estimated global inversion using 2D spline parameterization of the velocity field.

Discussion

This sequential procedure employs the best properties of each inversion technique and parameterization in the suitable stage of model knowledge. In the first inversion step, when there is no knowledge about the model, the data space is reduced (by layer stripping) and a kinematically equivalent model is estimated. In this step the 1D spline laterally velocity parameterization is used for each layer. It makes the inversion process more stable, there is no need of regularization, and it delivers very good structural results (Figure 4) compared to the original model at Figure 3.

Then, with the expected behavior of the velocity field in the real media, the parameterization is changed to compute the expected geological behavior. When using the layer stripping inversion in the second step, the effect of compaction is represented by equation 4. This choice is a (implicit) regularization by the model parameterization.

The global inversion also takes the benefits of the sequential tomographic inversion. Because the structural framework and the kinematic behavior are estimated in the first step, the global inversion tends to be closer to the solution and the chances to be trapped in a local minimum are reduced.

Both, layer stripping and global inversions give compatible results when they are used in the second tomographic step as the residuals, errors and geological incoherence index are reduced. As the GII for the original model is 6.45, for these examples the global approach gives slightly better results.

Conclusions

We present the Geological Incoherence Index and propose its use for the analysis, evaluation of inversion results, and, not described in this paper, to be added in the functional.

Sequential tomographic inversion evaluated with GII in two steps is presented. It is shown that it is robust for estimation of geologically feasible models without any need of explicit regularization. Layer-stripping with top-concordant layer parameterization, and global 2D splines discretization for the entire model, were tested as the second tomographic step. The second gives slightly better results.

Acknowledgments

To Petrobras.

References

BERKHOUT, A. J., 1997a, Pushing the limits of seismic imaging, part i: Prestack migration in terms of double dynamic focusing: Geophysics, 62, 937–954.

CARMICHAEL, R. S., 1982, Handbook of physical properties of rocks v.2: CRC Press, 2.

MAVKO, G., T. MUKERJI, and J. DVORKIN, 2009, The rock physics handbook. tools for seismic analysis of porous media: Cambridge University Press.

PARK, R. G., 1997, Foundations of structural geology: Chapman and Hall.

SEN, M. K., 2006, Seismic inversion: Society of Petroleum Engineers.

SHERIFF, R. E., 2002, Encyclopedic dictionary of exploration geophysics: Society of Exploration Geophysicist, 1.

SKINNER, B. J., and S. C. PORTER, 1987, Physical geology: Wiley.

THOMAS, J. E., 2000, Velocidades sismicas: Petrobras.